Transaction B: Mechanical Engineering
Vol. 17, No. 6, pp. 419–432

SCIENTIA IRANICA

Effect of Different Configurations on 3-D Analysis of Flow Through Stay Vanes and Guide Vanes of a Francis Turbine

R. Dadfar[1], B. Firoozabadi[1,*] and G. Ahmadi[2]

Abstract. *Stay and guide vanes (distributor) are essential parts of a turbine. They are used to control the flow rate and to appropriately transfer the flow momentum to the runner. In this work, flow through the distributor is analyzed. For various Boundary Conditions (BC) and different configurations, three-dimensional flows in the distributor of a Francis turbine are evaluated and compared with each other. The numerical simulations were carried out using Fluent software and the results were validated with a GAMM Francis turbine, where the geometry and detailed best efficiency measurements were publically available. In these simulations, the flow was assumed to be steady and the effect of turbulence was included using the $k-\varepsilon$ turbulence model. The study showed that an accurate prediction of velocity and pressure fields through the distributor may be obtained by considering a representative runner chamber with a single passage, including one blade of a stay and guide vane configuration. Furthermore, the corresponding needed computational resources for such an analysis are quite modest.*

Keywords: *Francis turbine; Stay vane; Guide vane; 3-D simulation.*

INTRODUCTION

The ever increasing demand for energy consumption requires the discovery of new energy resources and necessitates optimized use of currently available resources. Hydro-power energy is one of the most valuable energy sources due to its low carbon pollution foot print and its significance in managing water resources.

Generally, in a hydro-turbine, the flow enters the stay and guide vanes (distributor) after passing through a spiral casing. Stay vanes are used to stabilize the flow regime and generate appropriate swirl, and the guide vane directs the flow into the turbine runner at the desired angle. Guide vanes are also used to control the flow rate and, consequently, the power generated by the turbine. The appropriate direction of flow from the guide vane into the runner plays a critical role in turbine efficiency, and an inappropriate angle can result in significant losses in turbine performance. While earlier studies in turbine design were mainly experimental, the high cost of experimental investigation and increase in computational power has made numerical simulations studies of flows in turbomachinery quite attractive in recent years.

In the 1980's, Vu et al. [1] reported the numerical simulation of flow through the distributor using a two-dimensional computational domain. Later, developments in computer software and hardware made the simulations of three-dimensional flow in turbomachines possible, yet the numerical simulation of the entire turbine was not feasible. In 1994, Ruprecht et al. [2] investigated the flow field in a Francis turbine considering separate geometries of spiral casing, stay vanes and guide vanes. To have a more realistic inlet boundary condition, Ohishi et al. [3] used a computational domain for the spiral casing, which included containing the stay vanes. In a related work, an attempt was made to use guide vane geometry with a runner chamber in order to study flow in the distributor of a Francis turbine [4].

To evaluate the applicability of the standard $k-\varepsilon$ turbulence model for predicting hydrodynamic losses in the flow passage of a Francis turbine, Cherny et al. [5] used a configuration including one inter-blade channel of a guide vane and runner, with and without

1. *School of Mechanical Engineering, Sharif University of Technology, Tehran, P.O. Box 11155-9567, Iran.*
2. *Mechanical & Aeronautical Engineering, Clarkson University, P.O. Box 5725, Potsdam, NY, 13699-5700, USA.*
*. *Corresponding author. E-mail: firoozabadi@sharif.edu*

Received 22 May 2009; received in revised form 26 June 2010; accepted 3 October 2010

a draft tube. This configuration was also used to simulate flow-structure interaction in [6]. In 2009, Prasad et al. [7] used a configuration including one inter-blade channel of a stay vane, a guide vane and a runner with a draft tube, to study flow characteristics and performance parameters though a Francis Turbine using quasi and full 3-D approaches. To study the hydrodynamic performance of a Francis turbine, Oh and Yoon [8] used a configuration consisting of 24 blades of stay and guide vanes and a runner with 13 blades. Muntean et al. [9], in a related work, attempted to simulate the entire turbine from the inlet of the spiral casing to the outlet of the runner. Additional attempts also were made to simulate a complete Francis turbine using parallel processing techniques in [10-12].

While the simulation of an entire turbine is possible, the corresponding need for computational resources is prohibitively high. The goal of this paper is to develop an optimum representative configuration, together with appropriate boundary conditions, for simulating flow in a Francis turbine with desirable numerical accuracy, but with modest computational resources. We investigated several representative computational domains and different boundary conditions for analyzing flow in the stay and guide vanes of a GAMM (Gesellschaft fur Angewandte Mathematik und Mechanik) Francis turbine. The numerical results are validated with the experimental measurements for the GAMM turbine reported in [13-15].

GAMM FRANCIS TURBINE

The GAMM Francis turbine corresponds to a medium/high specific speed turbine. It was designed at the Institute of Hydraulic Machines and Fluid Mechanics (IMHEF) for experimental research in the hydraulic laboratory. The model was used as a test case in the 1989 GAMM workshop where all the geometrical information including stay vanes, guide vanes, runner, draft tube and optimal efficiency measurements were reported [13].

The distributor had 24 stay vanes and 24 guide vanes, while the runner had 13 blades with the external diameter of 0.4 m and the reference radius of 0.2 m. The runner angular velocity and flow rate of this turbine under design conditions were 500 rpm and 0.372 m^3/s [13]. In Figure 1, a schematic view of the GAMM Francis turbine meridian section with main dimensions, as well as a sketch showing the survey axes that were used to measure the velocity and pressure fields, is presented.

NUMERICAL ANALYSIS

A three-dimensional turbulent flow model, based on Reynolds averaged Navier-Stokes equations in a Cartesian coordinate system, was used in the present simulations. The two-equation standard $k-\varepsilon$ model was used to account for the turbulence effects. Numerical simulations were performed using Fluent software where a finite volume method with a SIMPLEC algorithm for pressure-velocity coupling, a power law scheme as the convection discretization procedure and a collocated grid arrangement were applied. As a convergence criterion, the computations were continued until the normalized residuals decreased to less than 10^{-7} for all discretized equations.

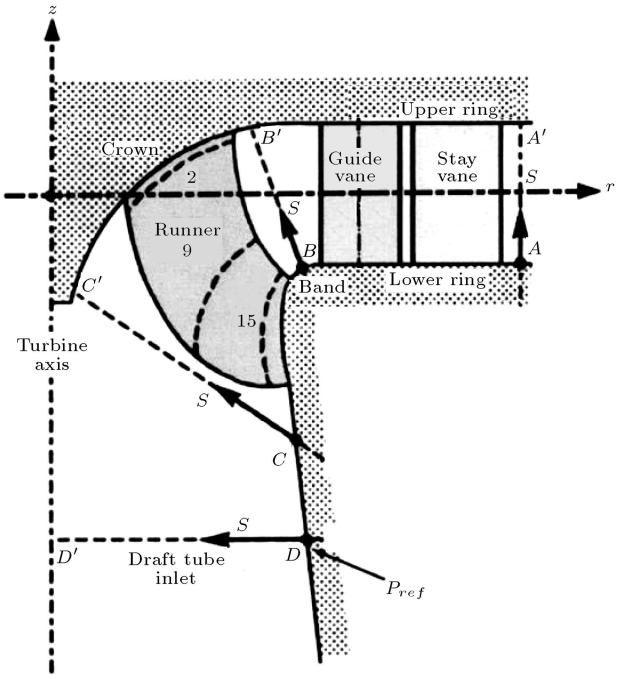

Figure 1. Meridian view of GAMM Francis turbine. z and r, respectively, are axial and radial axes [7].

GOVERNING EQUATION

The Reynolds-averaged continuity and Navier-Stokes equations for incompressible flows in a stationary reference frame were used in the analyses. These are:

$$\frac{\partial}{\partial x_i}(\rho U_i) = 0, \tag{1}$$

$$\frac{\partial}{\partial x_j}(\rho U_i U_j) = -\frac{\partial p}{\partial x_i} + \frac{\partial}{\partial x_j}\left[(\mu + \mu_t)\frac{\partial U_i}{\partial x_j}\right] + \rho g_i. \tag{2}$$

The standard $k-\varepsilon$ model for the transport of turbulence kinetic energy, k, and dissipation rate, ε, are:

$$\frac{\partial}{\partial x_i}(\rho k U_i) = \frac{\partial}{\partial x_i}\left[\left(\mu + \frac{\mu_t}{\sigma_k}\right)\frac{\partial k}{\partial x_i}\right] + G_k - \rho\varepsilon, \tag{3}$$

$$\frac{\partial}{\partial x_i}(\rho\varepsilon U_i) = \frac{\partial}{\partial x_j}\left[\left(\mu + \frac{\mu_t}{\sigma_\varepsilon}\right)\frac{\partial \varepsilon}{\partial x_j}\right] + C_{1\varepsilon}\frac{\varepsilon}{k}G_k - C_{2\varepsilon}\rho\frac{\varepsilon^2}{k}, \quad (4)$$

where:

$$G_k = \mu_t(2S_{ij}S_{ij}). \quad (5)$$

G_k, represents the production of turbulence kinetic energy due to the mean velocity gradient, and the mean strain rate is defined as:

$$S_{ij} = 1/2\left(\frac{\partial U_i}{\partial x_j} + \frac{\partial U_j}{\partial x_i}\right). \quad (6)$$

The turbulent (eddy) viscosity, μ_t, was computed from values of k and ε as:

$$\mu_t = \rho C_\mu \frac{k^2}{\varepsilon}. \quad (7)$$

Coefficients, $C_{1\varepsilon}$, $C_{2\varepsilon}$ and C_μ, are constants and σ_k and σ_ε are the turbulence Prandtl numbers for k and ε, respectively. The values of the constants are:

$$\sigma_k = 1.0, \qquad \sigma_\varepsilon = 1.3,$$
$$C_{1\varepsilon} = 1.44, \qquad C_{2\varepsilon} = 1.92, \qquad C_\mu = 0.09. \quad (8)$$

In the geometries with rotating parts (runner), Fluent software allows one to use a moving reference frame, using either absolute velocity, $\vec{U} = (U_x, U_y, U_z)$, or relative velocity, $\vec{U}_{rel}$, as the dependent variable. The two velocities are related by the following equation:

$$\vec{U}_{rel} = \vec{U}(\vec{r}) - (\vec{\Omega} \times \vec{r}), \quad (9)$$

where $\vec{\Omega}$ is the angular velocity vector (that is the angular velocity of the rotating frame), $\vec{r}$ is the position vector in the rotating frame and $\vec{\Omega} \times \vec{r}$ is the centrifugal acceleration. Finally, using relative velocity formulation, the left side of the momentum Equation 2 in a vector notation reads:

$$\Delta.(\rho\vec{U}_{rel}\vec{U}_{rel}) + \rho(2\vec{\Omega} \times \vec{U}_{rel} + \vec{\Omega} \times \vec{\Omega} \times \vec{r}), \quad (10)$$

where $\rho(2\vec{\Omega} \times \vec{U}_{rel})$ is the centrifugal force [16].

COMPUTATIONAL DOMAIN

Since simulation of the entire Francis turbine requires tremendous computational effort, for design purposes, it is advantageous to separately model different components of the turbine. In this case, selecting an appropriate representative configuration and specifying appropriate Boundary Conditions (BC) are crucial in the success of these simulations. In this paper, to investigate the effects of the computational domain, six different configurations, as shown in Figures 2 and 3, were studied. In Figure 2, the details of configuration 1 including its top and three-dimensional views together with its location in the distributor are depicted, while in Figure 3, the three-dimensional views of all six configurations are presented. The specifications of these configurations are:

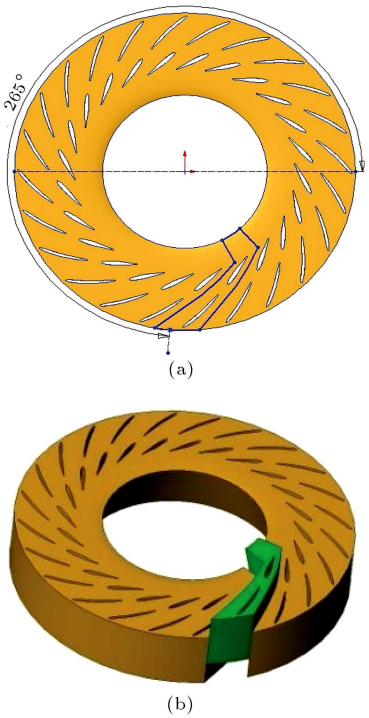

Figure 2. Geometrical details. (a) Top view of 1/24 cut of GAMM distributor used to build configuration 1. (b) Three-dimensional view of configuration 1 extracted from the distributor.

1. Configuration 1: Consists of a single passage, including one stay vane and one guide vane, which has a cut of 1/24 of the runner at the end.
2. Configuration 2: Consists of a single passage, including one stay vane and one guide vane, which has a cut following the velocity field.
3. Configuration 3: Consists of a single passage between two stay vanes and guide vanes.
4. Configuration 4: Consists of a single passage, including one stay vane, one guide vane and a runner chamber, which is prolonged to $z = -607.8$ mm.
5. Configuration 5: Consists of a single passage, including one stay and one guide vane, plus one inter-runner blade belonging to the Francis turbine, having 12 blades and which is prolonged to $z = -607.8$ mm.
6. Configuration 6: Consists of 24 stay and guide vanes, including the runner chamber, which is prolonged to $z = -607.8$ mm.

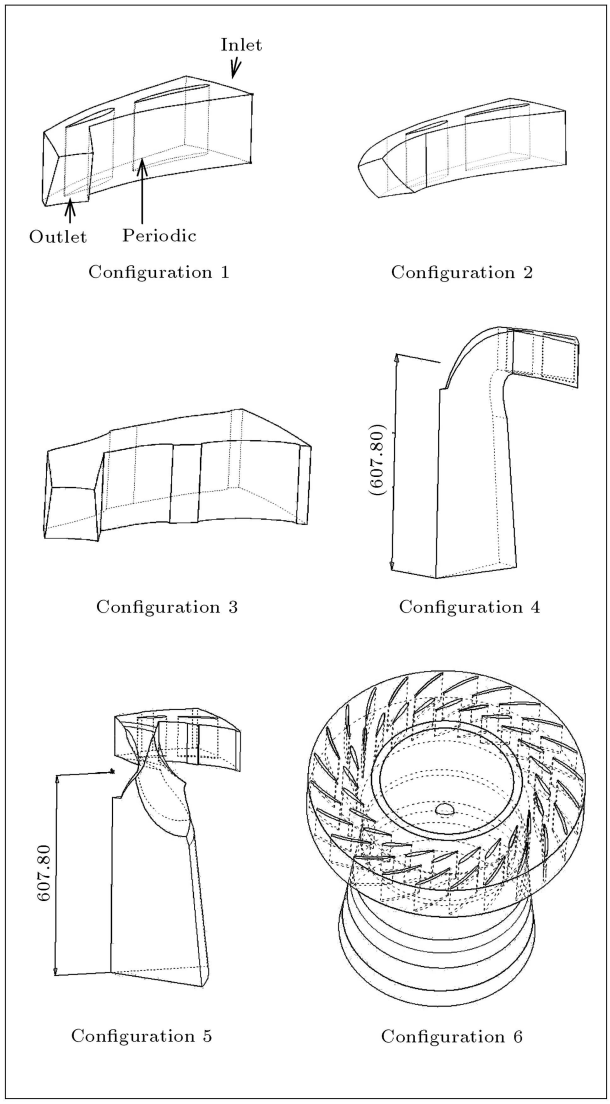

Figure 3. Different configurations used in the flow analyses.

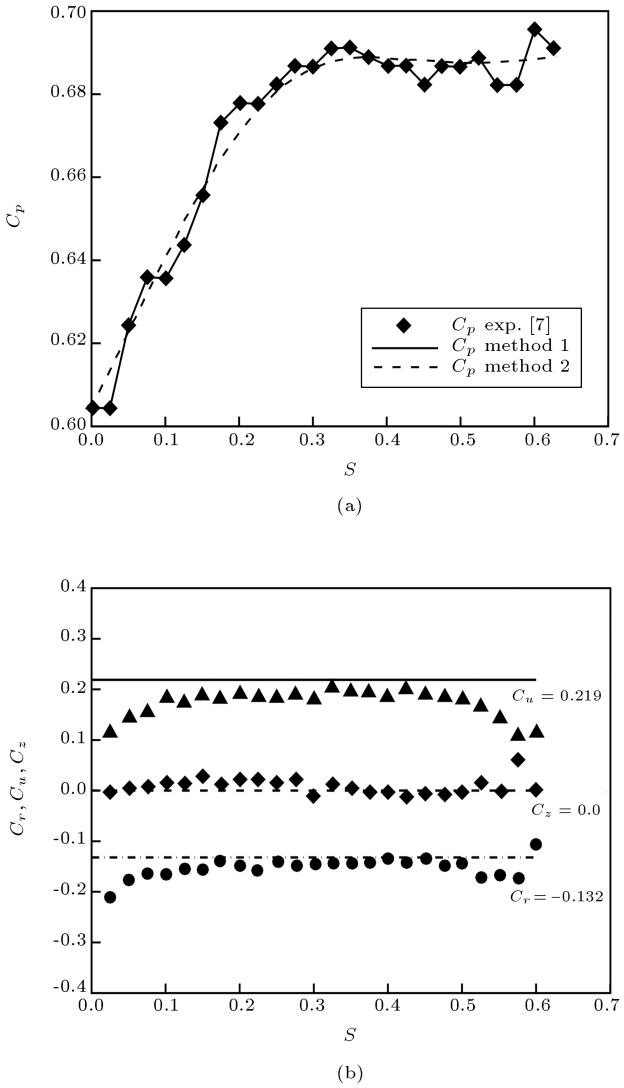

Figure 4. Distribution of velocity and pressure coefficients versus normalized abscissa (s) at section BB' for configuration 1. (a) Distribution of experimental and uniform inlet velocity coefficients; (b) Distribution of experimental pressure coefficient.

BOUNDARY CONDITIONS

To study the effects of various boundary conditions on the numerical simulation figuration 1 was selected for detailed analysis. This configuration includes a single passage of stay and guide vane, as shown in Figure 2, with periodic side surfaces in such a way that the vanes are in the middle of the computational domain. Furthermore, the inlet and outlet surfaces of the geometry were obtained by rotating the line segment AA' and BB' (shown in Figure 1) around the axis of symmetry by 360-degrees. Finally, the upper and lower surfaces were considered as part of the distributor ring. To investigate a suitable inlet boundary condition, experimental and uniform velocity distributions were applied at the inlet of configuration 1, as depicted in Figure 4a. The experimental velocity profiles at the inlet of the stay vane and hence at the outlet of the spiral case were measured in three different cross sections. These sections were placed along the peripheral direction (θ) with various angles, including 176, 265 and 355 degrees. The experimental measurements revealed that the velocity profiles along these angles were not identical, which might be a consequence of a non-ideal spiral case. Therefore, in the present analysis, the experimental velocity at 265 degrees was adopted as an inlet boundary condition [17]. According to Figure 4a, the experimental velocity coefficients at 265 degrees are not uniformly distributed throughout section AA', and decrease at both ends. This is a consequence of spiral casing and fluid viscous effects. The uniform velocity coefficient is also illustrated in Figure 4a. This was achieved by considering an ideal spiral casing. In this case, the inlet velocity vector was considered

to be tangent to the inlet of stay vanes throughout the system. Therefore, the magnitude of the radial velocity component was computed by dividing the flow rate, 0.372 m^3/s, by the inlet area, 0.2609 m^2. The circumferential velocity component was considered in such a manner where the fluid flow properly approaches the stay vanes (tangentially). Finally, for an ideal spiral casing, a zero axial velocity component was considered. These boundary conditions were used earlier by Muntean et al. [9]. The advantage of uniform velocity distribution is that this boundary condition can be specified based on general turbine data. At the outlet of the domain, four types of boundary condition were applied, three of which assumed some pressure distributions. As a first case, an experimental axisymmetric pressure distribution was applied (method 1 - Figure 4b). In another attempt, a smooth curve fitted on experimental data was used (method 2 - Figure 4b). As a third case, a uniform pressure distribution, using an average of experimental pressure measurements, was implemented ($C_P = 0.670$). Finally, a fully developed flow boundary condition at the outlet was applied. At the lateral surface of the domain, a periodic boundary condition was used and for the upper and lower parts of the distributor, the no-slip wall boundary condition was prescribed. In summary, five combinations of boundary condition were applied, which are as follow:

1. Experimental velocity distribution at the inlet, as shown in Figure 4a, and experimental pressure distribution (profile 1 in Figure 4b) at the outlet. (Note that the experimental velocity profile was measured at a section at an angle of 265 degree.)
2. Uniform velocity distribution at the inlet, as shown in Figure 4a, and experimental pressure distribution (profile 1 in Figure 4b) at the outlet.
3. Uniform velocity distribution at the inlet and a curve fitted to the experimental pressure distribution (profile 2 in Figure 4b) at the outlet.
4. Uniform velocity distribution at the inlet and uniform pressure distribution at the outlet.
5. Uniform velocity distribution at the inlet and fully developed flow assumption at the outlet.

In Figure 5, simulation results for the inlet pressure coefficient distribution, using a first and second set of boundary conditions, are presented. The predicted pressure coefficient for the first boundary condition is 2% higher than the experimental results. This difference may originate from the fact that the velocity distribution in the peripheral direction along the spiral casing is not completely uniform and, as was previously noted, the experimental velocity distribution used as the inlet condition was measured at a section at an angle of 265 degrees.

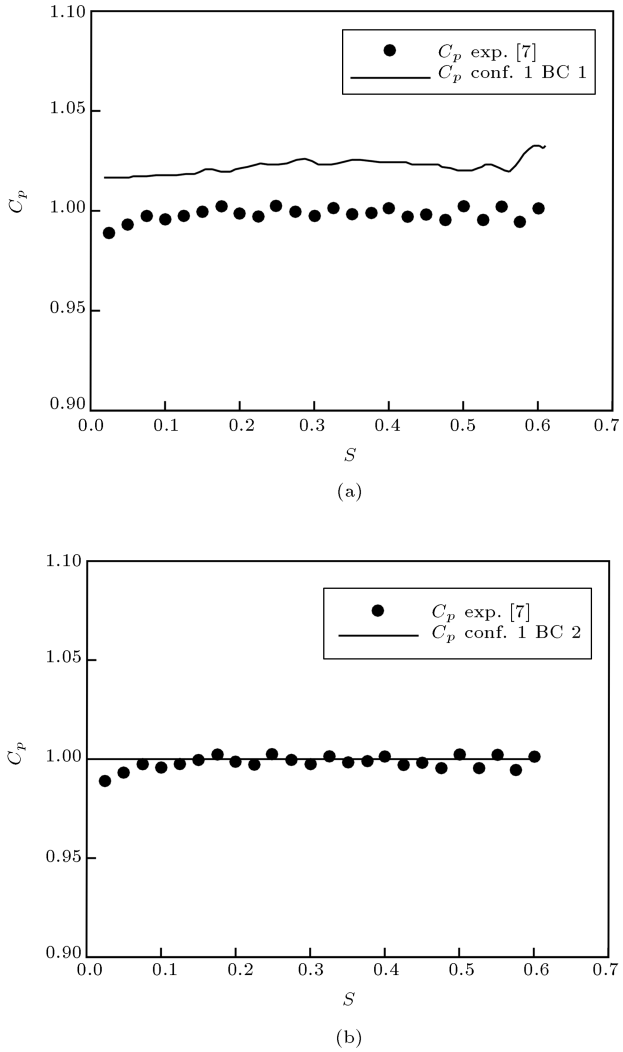

Figure 5. Distribution of pressure coefficient at section AA' for configuration 1. (a) Using first boundary conditions. (b) Using second boundary conditions.

In Figure 6a, the predicted outlet radial, axial and circumferential velocity coefficients for type 1 boundary conditions are presented. It is seen that, except near the casing, the present numerical results for the velocity coefficients are in agreement with the experimental data. In particular, the simulated circumferential velocity coefficient is in excellent agreement with the experimental data throughout section BB'. The radial velocity coefficient has an increasing trend toward the top of the section and is close to the measurement, except near the casing. The numerical predictions for the axial velocity coefficient have a satisfactory agreement with experimental data except at the lower part where the discrepancy is related to the curvature of the passage.

Due to the significance of the angle between the flow velocity vectors and the runner blades, the distribution of the outlet flow angle (α), which is defined as the angle between the velocity vector and its

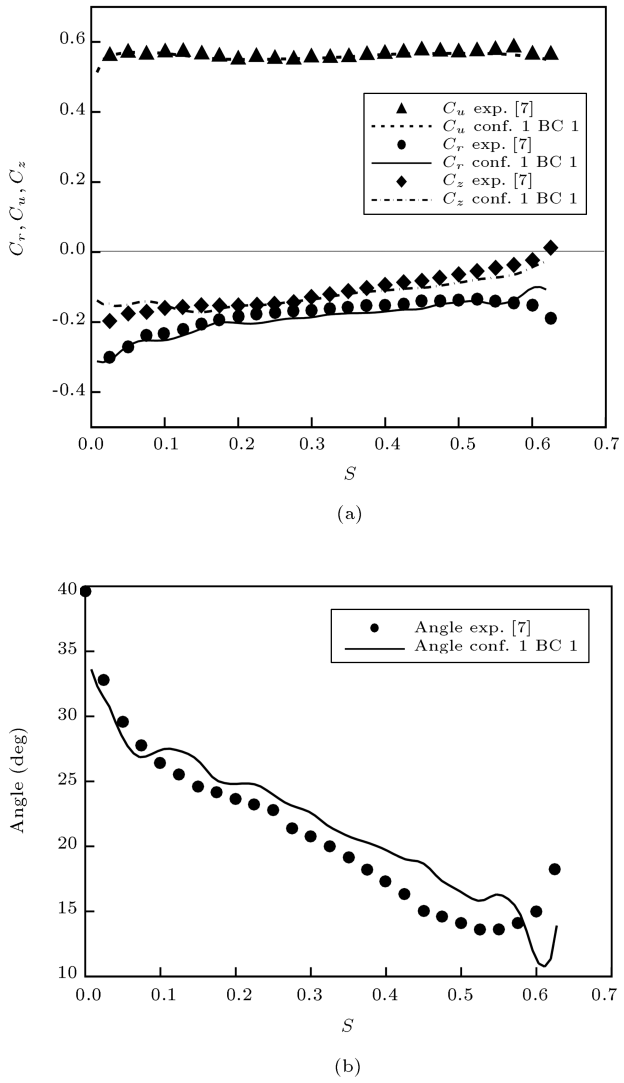

Figure 6. Distribution of velocity coefficients and flow angle at section BB' in configuration 1 for first boundary conditions. (a) Axial, circumferential and radial velocity coefficients. (b) Flow angle distribution.

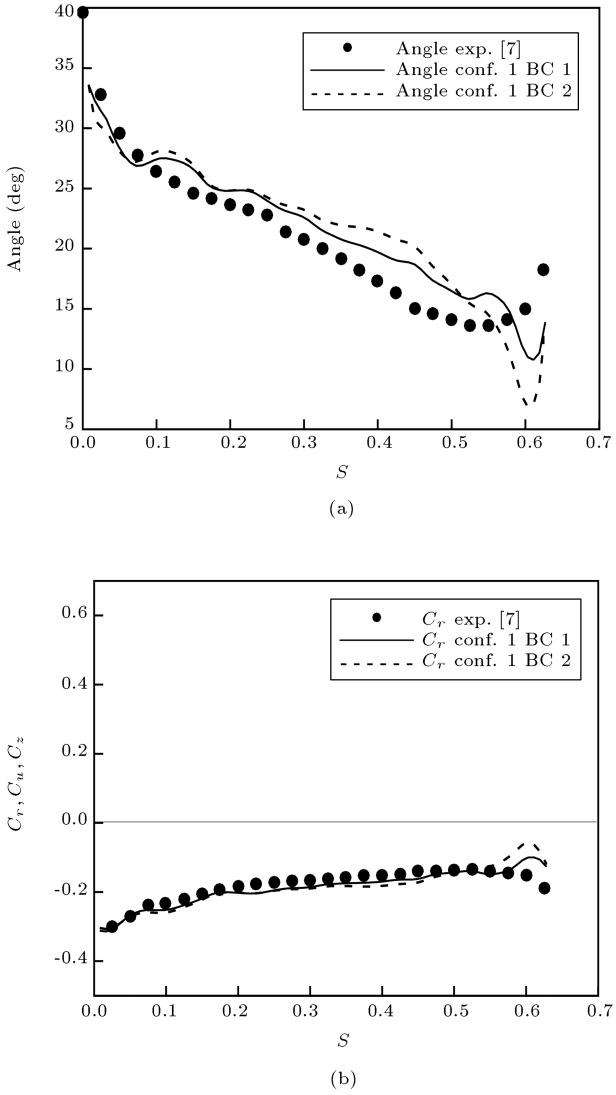

Figure 7. Distribution of flow angle and radial velocity coefficient at section BB' in configuration 1 using first and second boundary conditions. (a) Flow angle distribution. (b) Radial velocity coefficient.

circumferential component, is presented in Figure 6b. Although the predicted magnitude of the flow angle is slightly higher than the experimental data, the trend of behavior is close to the experiments. This figure also shows that near the upper part of the section, there is a decrease in the flow angle, which is recovered toward the wall. It is conjectured that this trend is due to an increase in local pressure.

To compare the effect of various inlet velocity profiles, the outlet flow angle and the radial velocity coefficients obtained by the use of first and second boundary conditions are presented in Figures 7a and 7b. It is seen that, in both cases, the numerical results follow the same trend. However, when using second boundary conditions, deviation between the predicted radial velocity coefficient and the experimental measurement increases. In addition, the outlet flow angle is also predicted with slightly less precision when compared with the use of the first set of boundary conditions.

Figure 8a shows the distributions of the outlet flow angle using the first and third boundary conditions. It is seen that for both cases, the numerical trends are similar. However, since for the third boundary condition, the prescribed outlet pressure was obtained by smoothing the experimental data by use of a polynomial regression, the resultant flow angle is smoother compared to experimental measurement.

In Figure 8b, the distributions of the outlet flow angle as predicted by the use of the first and fourth set of boundary conditions are presented. This figure shows that using the fourth boundary condition, which assumes a uniform outlet pressure, leads to inaccurate

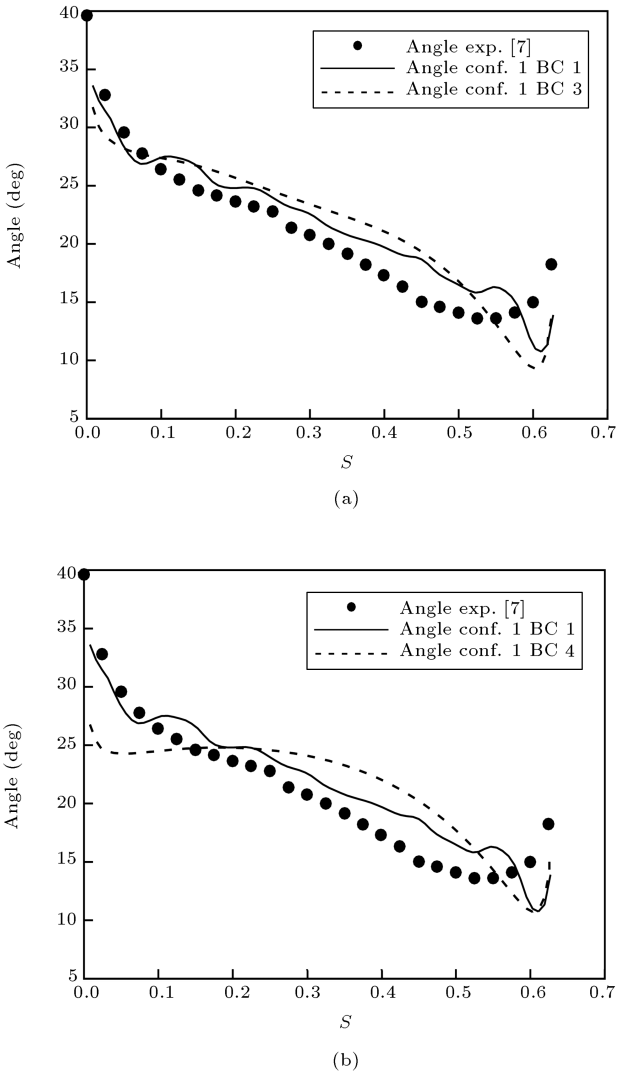

Figure 8. Flow angle distributions at section BB' for configuration 1. (a) Using first and third boundary conditions. (b) Using first and forth boundary conditions.

results, and the predicted flow angle deviates significantly from experimental data.

In summary, the simulations results show that using a uniform velocity profile at the inlet leads to accurate prediction of the outlet flow angle distribution (at section BB'). This will provide the opportunity to simulate the flow field in the distributor of a Francis turbine, without inclusion of the spiral casing with reasonable accuracy. Thus, in the subsequent section of this paper, we used the following boundary conditions.

Inlet

A uniform velocity field was prescribed at the inlet of computational domains [8]. The radial component of the inlet velocity was computed by dividing the total flow rate (0.372 m^3/s) by the inlet cross sectional area. The axial velocity component was assumed to be zero; assuming a perfect spiral casing. The circumferential velocity component was evaluated based on the assumption that the inlet velocity vectors are parallel to the stay vane blades (with angle $\gamma = 340$). The turbulence intensity, I (the ratio of the root-mean-square velocity fluctuations to the mean flow velocity), and turbulence length scale, ℓ, were assumed, respectively, to be 8% and 0.02 m. The turbulence kinetic energy, k, and dissipation rates, ε, are then given as [16];

$$k = \frac{3}{2}\left(u_{\text{avg}} I\right)^2, \tag{11}$$

$$\varepsilon = C_\mu^{3/4} \frac{k^{3/2}}{\ell}, \tag{12}$$

where u_{avg} is the mean flow velocity and C_μ is an empirical model constant.

Outlet

In configurations 1, 2 and 3, the experimental pressure profile was prescribed at the outlets and in the rest of the computational domains, a fully developed outlet velocity was assumed. This condition enforces zero normal gradients for all flow variables except pressure.

Periodic

For configurations 1 through 5, the periodic boundary conditions were imposed on the side boundaries. That is;

$$\vec{V}(r,\theta,z) = \vec{V}\left(r, \theta + \frac{2\pi}{n}, z\right),$$

$$p(r,\theta,z) = p\left(r, \theta + \frac{2\pi}{n}, z\right), \tag{13}$$

where n is the number of circumferential parts of the entire turbine ($n = 24$).

Wall

The no-slip boundary condition (zero velocity relative to the boundary) was imposed on the walls and the near wall treatment was performed using a switching method based on y^*. It should be noted that in Fluent, the laws-of-the-wall for mean velocity are based on wall unit, y^*, rather than $y^+ (= \rho u_\tau y/\mu)$. These quantities are approximately equal in equilibrium turbulent boundary layers [16,18] and y^* is defined as follows:

$$y^* = \frac{C_\mu^{1/4} k_p^{1/2} y_p}{\mu}, \tag{14}$$

where k is the von Karman constant ($= 0.4187$) and y_p is the distance from grid point p to the wall.

For $y^* > 11.25$, the log law of the wall was used:

$$u^* = \frac{1}{k}\ln(Ey^*), \tag{15}$$

in which E is an empirical constant ($= 9.793$) and the shear velocity is given as:

$$u^* = \frac{u_p C_\mu^{1/4} k_p^{1/2}}{\tau_\omega/\rho}. \tag{16}$$

Here, k_p and u_p are turbulence kinetic energy and mean velocity at point p.

When the mesh was such that $y^* < 11.25$ at the wall-adjacent cells, the linear viscous sublayer velocity was applied [16], that is:

$$u^* = y^*. \tag{17}$$

VALIDATION OF THE COMPUTATIONAL RESULTS

Grid Independency

To confirm the grid independency of the present simulations, three grid sizes (46,000, 265,000 and 443,000 nodes) for configuration 1 were used. The computational domain was discretized using the structured boundary layer mesh, as shown in Figure 9a. Furthermore, for the near wall treatment, the average of y^* near the wall was 39 (y^+ of 40) and the majority of y^+ near the stay and guide vanes were kept at around 35 wall units, as recommended by the Fluent users' manual [16]. Figure 9b shows the predicted distributions of flow angle for these different grids. For the coarse grid of 46,000 nodes, the flow angle distribution is different from the other two more refined grids. Therefore, the mesh of 265,000 nodes was used to discretize the computational domain for configuration 1, which includes a single passage containing one blade of stay and one guide vane. In the same manner, the meshes for the other configurations were also tested to make sure the results were grid independent.

SELECTION OF AN OPTIMUM CONFIGURATION WITHOUT THE RUNNER CHAMBER

Configurations 1 and 2

These two configurations consist of a single passage including one blade of stay and a guide vane with different end cuts. In configuration 1, the end is obtained by cutting 1/24 of the runner chamber, while in configuration 2, the end follows the velocity field.

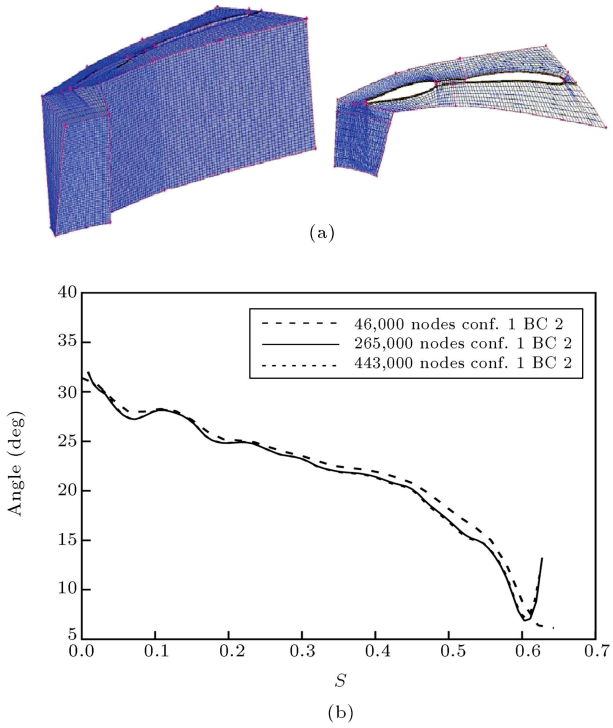

Figure 9. Computational mesh and flow angle distribution at section BB' in configuration 1. (a) Structural body fitted coordinate grid. (b) Flow angle distribution using second boundary conditions.

In Figure 10, velocity coefficients for the first and second configurations are plotted. For both these configurations, the predicted circumferential, radial and axial velocity coefficients are close to experimental measurements across section BB', except near the upper and lower part of the casing (Figure 10a and 10b). Figure 10a shows that the predicted axial velocity coefficient deviates from the experimental measurement, while Figure 10b shows that more realistic results were obtained using configuration 1. Therefore, it is concluded that the predicted velocity fields for configuration 1 were slightly more accurate when compared with those of configuration 2. However, there are practically negligible differences between these results.

Configurations 1 and 3

Configuration 3 consists of a single passage between a blade of stay and a guide vane, and includes a cut of 1/24 of the runner chamber at the end. In Figure 11, the radial, circumferential and axial velocity coefficients at section BB' for configurations 1 and 3 are compared. Although distributions of radial and axial velocity coefficients are almost the same (as seen in Figure 11b), the circumferential velocity coefficient for configuration 3 is lower than that of configuration 1 and experimental measurements

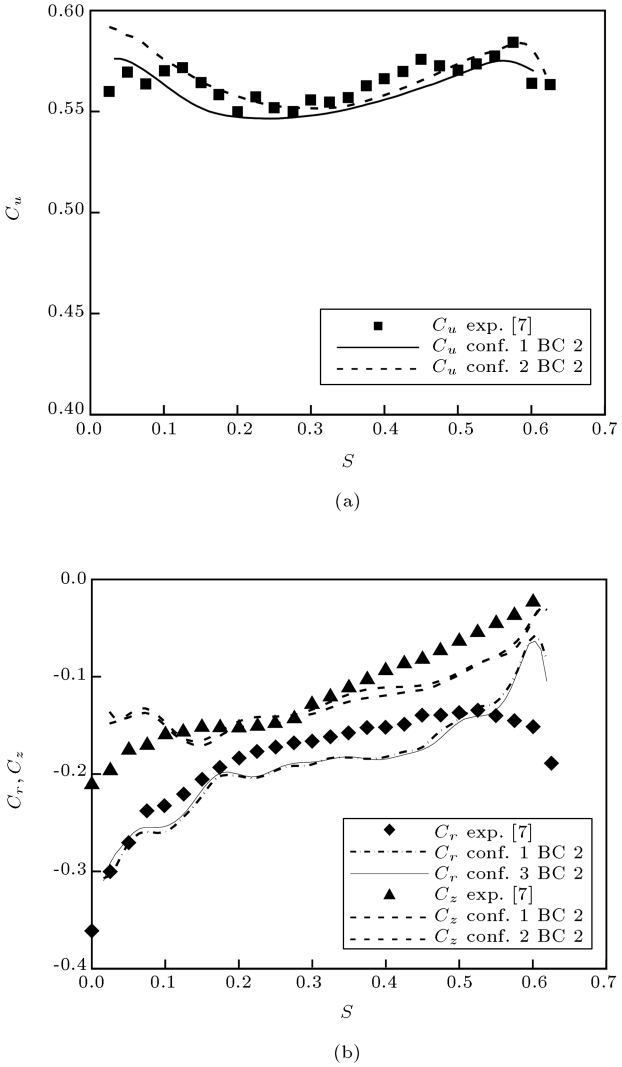

Figure 10. Distribution of velocity coefficients at section BB' for configurations 1 and 2. (a) Circumferential velocity coefficients. (b) Radial and axial velocity coefficients.

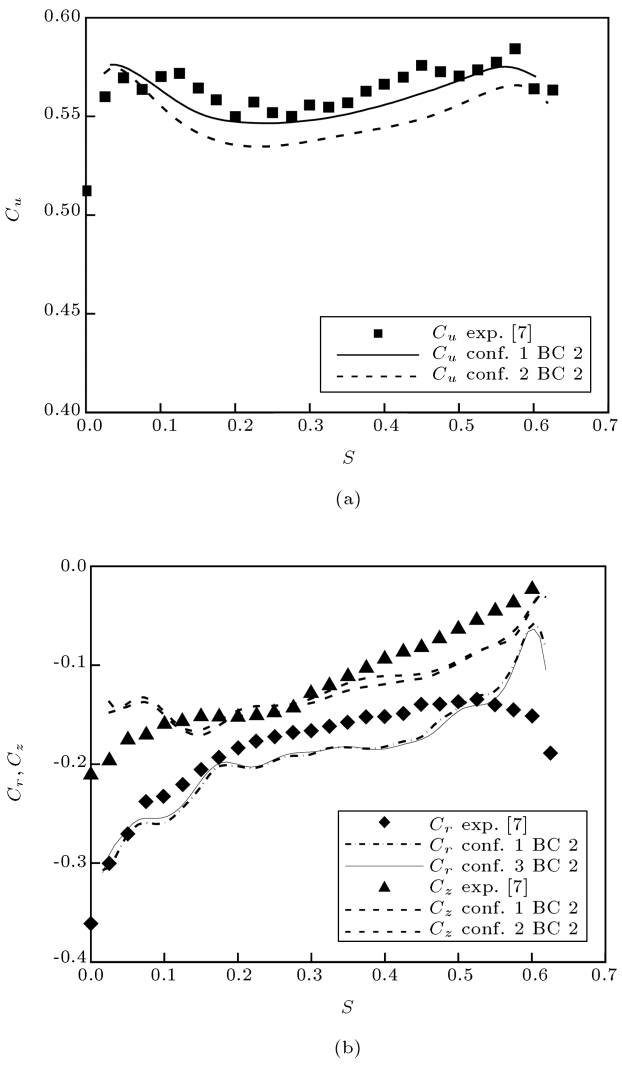

Figure 11. Distribution of velocity coefficients at section BB' for configurations 1 and 3. (a) Circumferential velocity coefficient. (b) Radial and axial velocity coefficients.

(as seen in Figure 11a). Therefore, although using configuration 1 seems to lead to a slightly better prediction, there are no noticeable differences between these results.

From the above comparisons, it is concluded that configuration 1 is slightly more suitable than the other configurations. However, since there are no major differences between the results, configurations 1, 2 or 3 may be used for analysis of flow through the distributor of a Francis turbine, depending on available conditions and requirements.

EFFECTS OF THE RUNNER CHAMBER ON FLOW ANALYSIS

In Figure 12, flow angle distributions for configurations 1 and 4 are compared. The maximum difference between the simulation results and the experimental

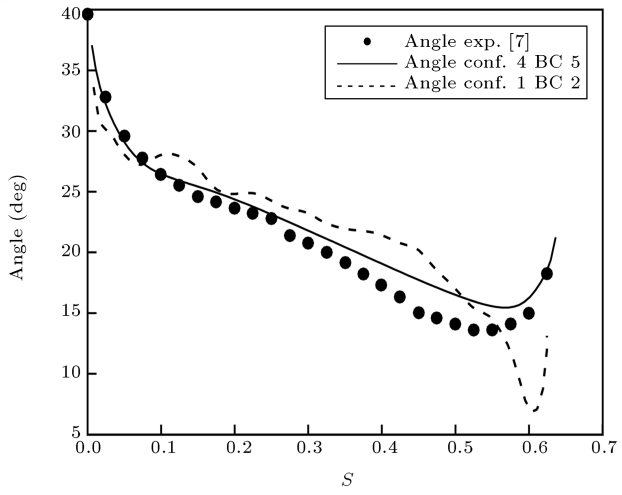

Figure 12. Flow angle distributions at section BB' for configurations 1 and 4.

data using configuration 1 is 9.4 degrees, while the difference is 2.6 degrees for configuration 4.

In Figure 13, distributions of velocity and pressure coefficients along section BB' for configuration 4 are shown. Figure 13a shows that the predicted pressure coefficient is in good agreement with the experimental data. Furthermore, the circumferential velocity coefficient across the BB' section was predicted accurately. The predicted radial velocity coefficient is similar to experimental measurements, except near the middle of the section. The axial velocity coefficient is also predicted accurately, except in a small area in the upper surface. In Figures 13c and 13d, flow angle and meridian velocity coefficients are presented. These figures show that the simulation results are in reasonable agreement with experimental data.

The results shown in Figure 13 indicate that the velocity and pressure fields can be more accurately predicted by using configuration 4, rather than configuration 1.

EFFECTS OF THE RUNNER BLADE ON PRESSURE DISTRIBUTION AROUND THE GUIDE VANE

In this section, the simulation results for configuration 5, which includes a passage between two runner blades, at an angular velocity of 500 rpm, are compared with the results for configuration 4. In Figure 14a, distributions of pressure coefficients on the pressure side of the stay vane are shown. It is seen that the pressure coefficient decreases along the cord, due to the increase in velocity from the tip to the tail of the blade. The same trend is observed for the suction side of the stay vane in Figure 14b. Comparison of Figures 14a and 14b reveals that the magnitude of

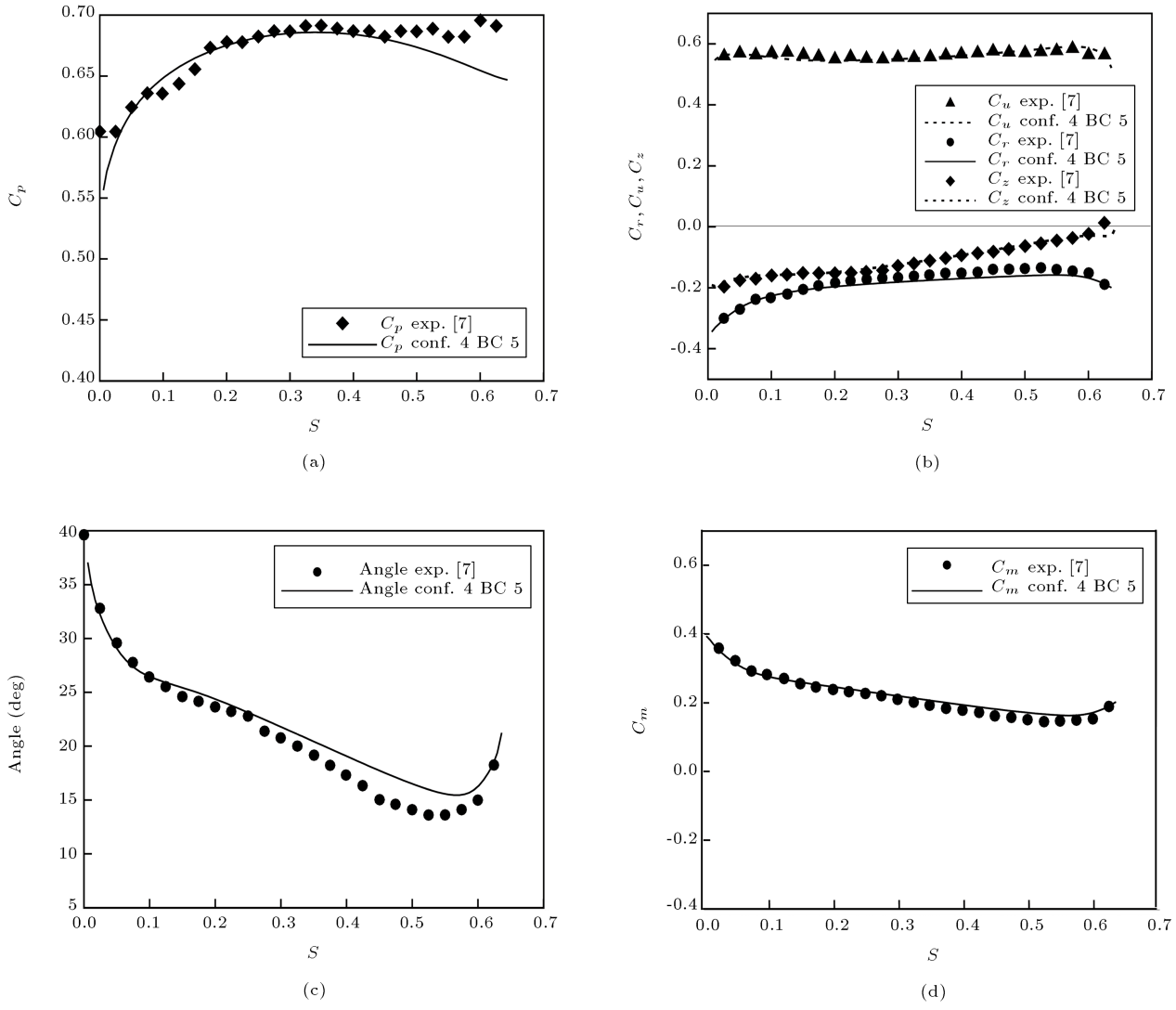

Figure 13. Distribution of velocity and pressure coefficients at section BB' for configuration 4. (a) Pressure; (b) circumferential, radial and axial velocity coefficients; (c) flow angle and (d) meridian velocity coefficient.

pressure coefficient on the suction side is less than that on the pressure side, as expected. It is also seen that there is no noticeable difference between the results of configurations 4 and 5.

In Figure 14c, distributions of pressure coefficients on the pressure side of the guide vane are presented. Near the tip of the blade, the pressure coefficient corresponds to the stagnation point at the leading edge. Since the runner acts as a wall in front of the flow, distribution of the pressure coefficient in configuration 5 (with runner blade) is slightly higher than that in configuration 4. In Figure 14d, the pressure coefficients on the suction side of guide vane are depicted. The results are similar for the two configurations, except near the trailing edge, where the decrease in the pressure coefficient is a consequence of the runner rotation. From the above discussions, it may be concluded that the runner blades under turbine design conditions have no significant effects on distribution of the pressure coefficient around the stay and guide vanes.

EFFECTS OF PERIODIC BOUNDARY CONDITION

For configuration 6, which is the entire system, a grid of 1,187,608 nodes was used. Thus, the grid is coarser compared with one for a segment of the turbine. Arriving at the same grid density requires a grid with about 6 million nodes.

The contours shown in Figures 15a and 15b are for equal flow angle related to configurations 4 and 6. In Figure 15a, the contour is on a surface resulting from a 360 degree rotation of BB' around the z axis (Figure 1), while in Figure 15b, it is on the outlet surface of configuration 4. In Figure 15b, the contours are symmetric, since the configuration and inlet velocity are symmetric. However, there are some disturbances

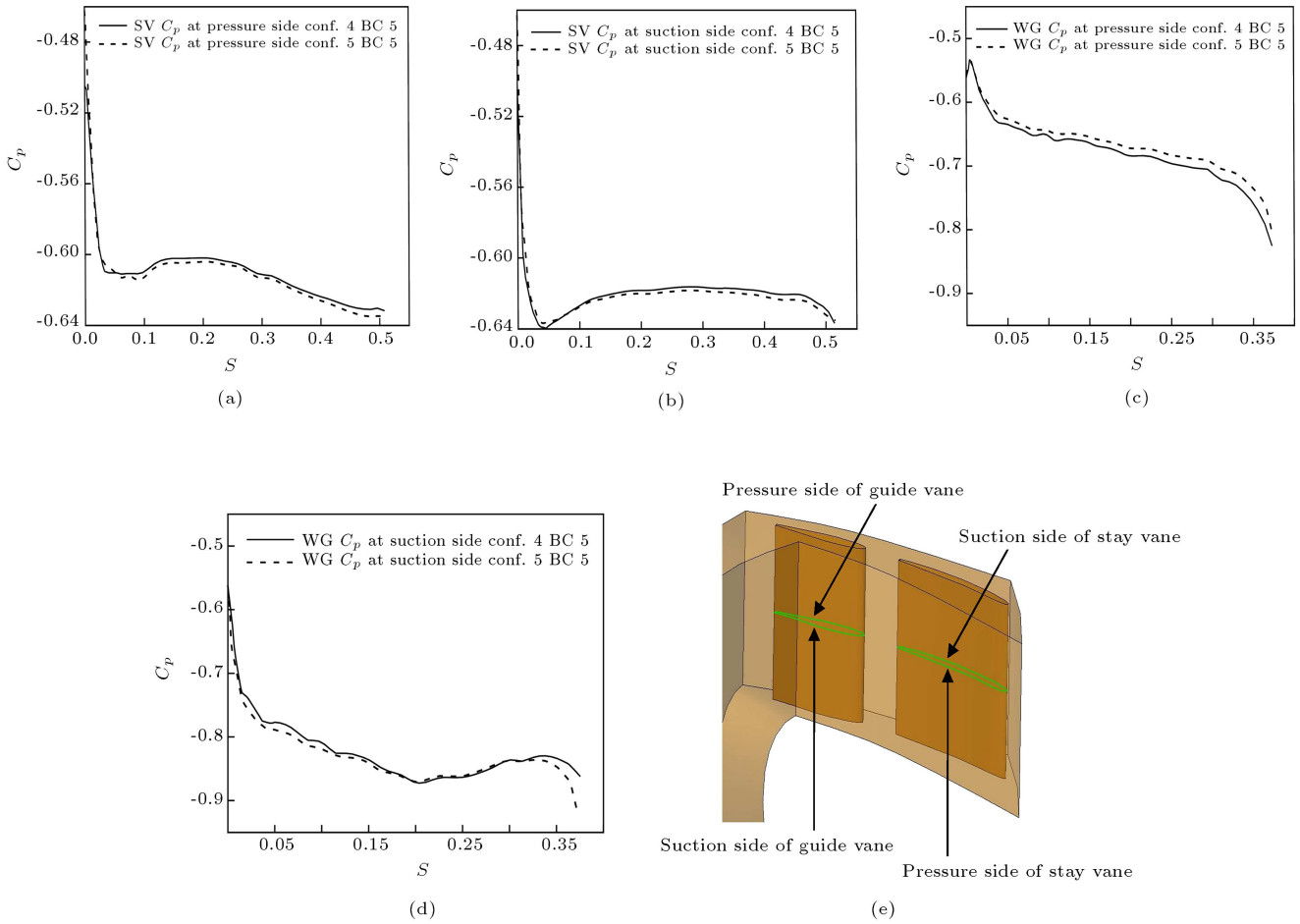

Figure 14. Distribution of pressure coefficient on stay and guide vane at section BB' for configurations 4 and 5 (the data is extracted from the outer periphery of the cross section located on one-half the height of the vanes). (a) Pressure coefficient on pressure side of stay vane. (b) Pressure coefficient on suction side of stay vane. (c) Pressure coefficient on pressure side of guide vane. (d) Pressure coefficient on suction side of guide vane. e- Pressure and suction side of stay and guide vanes.

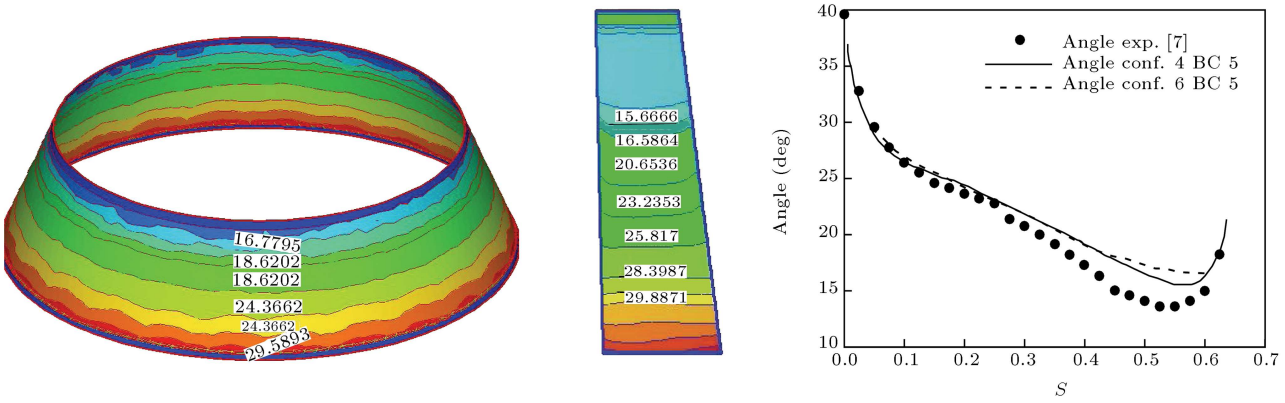

(a) Equal-flow angle contours for configuration 6

(b) Equal-flow angle contours for configuration 4

(c) Flow angle distribution for configurations 4 and 6 at section BB'

Figure 15. Flow angle distributions for configurations 4 and 6. (a) Equal-flow angle contours for configuration 6. (b) Equal-flow angle contours for configuration 4. (c) Flow angle distribution for configurations 4 and 6 at section BB'.

in the upper and lower parts of the axis, which may originate from the coarse grid. In Figure 15c, flow angle distributions for configurations 4 and 6 are compared. The slight difference (around 1 degree) between the two configurations is a consequence of the coarse grid in configuration 6.

As a result, the periodic boundary condition can be used safely for the analysis of flow in the distributor of a Francis turbine under design conditions.

CONCLUSIONS

In the present paper, different configurations and boundary conditions for simulating flow through a Francis turbine are investigated. The results for different boundary conditions for a representative segment of the turbine showed that it is possible to use a uniform velocity inlet boundary condition prior to stay vanes, despite the presence of the rather complex spiral casing. The acceptability of a uniform velocity boundary condition is significant, since it can be computed directly from the flow rate information of the Francis turbine.

The simulations also showed that adding the runner chamber at the outlet, together with a fully developed condition at the exit, leads to a better prediction of the velocity and pressure fields. To reduce the computational cost, it is also possible to analyze a representative segment of the turbine including one stay and guide vane, using periodic boundary conditions instead of the entire blades' configuration.

It is also shown that using different representative configurations of stay and guide vanes, as selected in the present study, leads to comparable results. Finally, it is revealed that the presence of runner blades under design conditions has minor effects on the pressure field around the stay and guide vane.

ACKNOWLEDGMENT

The authors would like to thank Farab Inc. for their financial and technical support of this research.

NOMENCLATURE

$\vec{r}$	position vector in rotating frame (m)
$\vec{U}$	absolute velocity vector (m/s)
$\vec{U}_{rel}$	relative velocity vector (m/s)
U_u	absolute circumferential velocity (m/s)
U_r	absolute radial velocity (m/s)
U_z	absolute axial velocity (m/s)
$U_m=\sqrt{U_r^2+U_z^2}$	absolute meridian velocity (m/s)
$C_u=U_u/\sqrt{2E}$	absolute circumferential velocity coefficient
$C_r=U_r/\sqrt{2E}$	absolute radial velocity coefficient
$C_z=U_z/\sqrt{2E}$	absolute axial velocity coefficient
$C_m=\frac{c_m}{\sqrt{2E}}=\sqrt{C_r^2+C_z^2}$	absolute meridian velocity coefficient
$C_p=\frac{(P-P_{ref})}{\rho E}$	pressure coefficient
$\vec{\Omega}$	angular velocity vector (1/s)
ρ	flow density (kg/m^3)
μ	dynamic viscosity (Ns/m^2)
g	acceleration due to gravity (m/s^2)
ℓ	turbulence length scale (m)

I	turbulence intensity
μ_t	turbulent viscosity (Ns/m^2)
k	turbulent kinetic energy (m^2/s^2)
ε	dissipation rate (m^2/s^2)
$E = gH$	specific hydraulic energy (J/kg)
H	net head (m)
P	static pressure (N/m^2)
Q	volume flow rate (m^3/s)
$R_{ref} = 0.2$ m	reference radius (m)
ref	inlet of draft tube
$s = \frac{\text{length}}{R_{ref}}$	normalized abscissa
$\alpha = \arctan\left(\frac{c_m}{c_u}\right)$	flow angle (degree)

REFERENCES

1. Vu, T.C., Shyy, W., Brarren, M.E. and Reggio, M. "Recent developments in viscous flow analysis for hydraulic turbine components", *13th IAHR Symposium*, Montreal (1986).
2. Ruprecht, A., Bauer, C. and Riedelbauch, S. "Numerical analysis of three-dimensional flow through turbine spiral case and wicket gates", *17th IAHR Symposium*, Beijing (1994).
3. Ohishi, H., Han, F. and Kubota, T. "3-D viscous flow in spiral case of a Francis turbine", *21th IAHR Symposium*, Lausanne (2002).
4. Suzuki, T., Nagafuji, T., Komiya, H., Shimada, T. "Flow behavior around stay vanes and guide vanes of a Francis turbine", *Journal of Fluids Engineering, Transactions of the ASME*, **118**(1), pp. 110-115 (1996).
5. Cherny, S.G., Chirkov, D.V., Lapin, V.N., Skorospelov, V.A. and Turuk, P.A. "Numerical simulation of a turbulent flow in the Francis hydroturbine", *Russian Journal of Numerical Analysis and Mathematical Modeling*, **21**(5), pp. 425-446 (2006).
6. Wang, W.Q., He, X.Q., Zhang, L.X., Liew, K.M. and Guo, Y. "Strongly coupled simulation of fluid-structure interaction in a Francis hydro turbine", *International Journal for Numerical Methods in Fluids*, **60**(5), pp. 515-538 (2009).
7. Prasad, V., Sayann, K.S. and Krishnamachar, P. "Quasi-3D and full-3D approaches for numerical simulation in an axial flow hydraulic turbine", *Journal of Water Energy and Environment*, **4**(4), pp. 42-48 (2009).
8. Oh, H.W. and Yoon, E.S. "Application of computational fluid dynamics to performance analysis of a Francis hydraulic turbine", *Proceedings of the Institution of Mechanical Engineers, Part A: Journal of Power and Energy*, **221**(4), pp. 583-590 (2007).
9. Muntean, S., Susan, R. and Anton, I. "3D flow analysis of the GAMM Francis turbine for variable discharge", *21th IAHR Symposium*, Lausanne (2002).
10. Carija, Z., Mrsa, Z. and Fucak, S. "Validation of Francis water turbine CFD simulations", *Strojarstvo*, **50**(1), pp. 5-14 (2008).
11. Carija, Z. and Mrsa, Z. "Complete Francis turbine flow simulation for the whole range of discharges", *4th International Congress of Croatian Society of Mechanics*, Bizovac (2003).
12. Ruprecht, A., Heitele, M., Helmrich, T., Moser, W. and Aschenbrenner, T. "Numerical simulation of a complete Francis turbine including unsteady rotor/stator interactions", *20th IAHR Symposium*, Charlotte (2000).
13. Parkinson, E. "Test case 8: Francis turbine", *Turbomachinery Workshop ERCOFTAC II*, Lausanne (1995).
14. Avellan, F., Dupont, P., Farhat, M., Gindroz, B., Henry, P., Hussain, M., Parkinson, E. and Santal, O. "Flow survey and blade pressure measurements in a Francis turbine model", *Proceedings of 15th IAHR Symposium*, Belgrade (1990).
15. Parkinson, E., Dupont, P., Hirschi, R., Huang, J. and Avellan, F. "Comparison of flow computation results with experimental flow surveys in a Francis turbine", *17th IAHR Symposium*, Beijing (1994).
16. Fluent Inc. Fluent 6.1 user's manual, Centerra Resource Park, Lebanon (2001).
17. Avellan, F., Dupont, P., Farhat, M., Gindrozm, B., Henry, P., Hussain, M., Parkinson, E. and Santal O. "Experimental flow study of the GAMM turbine model", *Proceedings of the GAMM Workshop*, Lausanne (1989).
18. Launder, B.E. and Spalding, D.B. "Numerical computation of turbulent flows", *Journal of Computer Methods in Applied Mechanics and Engineering*, **3**(2), pp. 269-289 (1974).

BIOGRAPHIES

Reza Dadfar received his B.S. degree in Mechanical Engineering (Fluid Mechanics) from Isfahan University of Technology and his M.S. degree in Mechanical Engineering (Energy Conversion) from Sharif University of Technology, Tehran. His research interests include: Application of CFD to Turbomachinery, Mechanisms of Flow Instability and Turbulence.

Bahar Firoozabadi received her Ph.D. in Mechanical Engineering from Sharif University of Technology, Tehran, where she is now Associate Professor in the Department of Mechanical Engineering. Her research interests include: Fluid Mechanics in Density Currents, presently focusing on Biofluid Mechanics, and Porous Media. She teaches Fluid Mechanics and Gas Dynamics to undergraduates, and Viscous Flow, Advanced

Fluid Mechanics, Continuum Mechanics and Biofluid Mechanics to graduate students.

Goodarz Ahmadi is a Clarkson Distinguished Professor, and Robert R. Hill Professor of Mechanical and Aeronautical Engineering at Clarkson University. He is also serving as the Dean of Engineering of the Coulter School of Engineering at Clarkson.

His research interests include: Particle Transport Deposition and Removal, Multiphase and Granular Flows, Active Flow Control, Turbulence, Flow through Porous Media, and Passive and Active Vibration Control. His research has been supported by the Environmental Protection Agency, Department of Energy, the National Science Foundation, NASA, Corning, IBM, Xerox, Dura Pharmaceutical, NYSTAR and AFOSR.

Professor Ahmadi has co-authored two books and over 470 technical publications in archival journals. He also has made more than 500 presentations at national and international technical meetings and has given more than 100 invited talks and short courses at other institutions. He is serving as a member of the Editorial Board and Editorial Advisory Board of seven international and national journals.

He is a Fellow of ASME, ISME and ISCE, and has received many awards.